Article:
Wu, L., Liu, X., Palamarciuc, I. et al. (2026) The bearing shell surface indentation and early-state wear detection combining active ultrasound and one-dimensional convolutional neural network. Wear, 591. 206592. ISSN: 0043-1648

https://doi.org/10.1016/j.wear.2026.206592

The Bearing Shell Surface Indentation and Early-state Wear Detection Combining Active Ultrasound and One-dimensional Convolutional Neural Network

Liqun Wu [a], Xianyuan Liu [b, c], Ion Palamarciuc [d*], Rizwan Bajwa [d], Yi Zhang [e], Rob Dwyer-Joyce [a*]

[a] *Leonardo Centre for Tribology, School of Mechanical, Aerospace and Civil Engineering, The University of Sheffield, Sheffield, S10 2TN, United Kingdom*

[b] *Centre for Machine Intelligence, School of Computer Science, The University of Sheffield, Sheffield, S1 3JD, United Kingdom*

[c] *School of Computer Science, The University of Sheffield, Sheffield, S1 4DP, United Kingdom*

[d] *Daido Metal Co., Ltd. European Technical Centre (UK), Ilminster, Somerset, TA19 9PH, United Kingdom*

[e] *Daido Metal Co., Ltd., Technology Division, Tendoh Shinden, Maehara, Inuyama, Aichi, 484-0061, Japan*

[*] *Corresponding authors: r.dwyer-joyce@sheffield.ac.uk & ion.palamarciuc@daidometal.com*

Abstract: High frequency ultrasound has been utilized for a long-term and in-situ wear monitoring of journal bearing coatings. However, during the actual operation, the wear scar and the surface profile always change dynamically, which can lead to an inaccurate result, especially at the early-stage of wear generation. In this article, the ultrasound behaviour of early-state wear is initially investigated by the numerical models. Then, the early-state wear is simulated through the indentation experiments of marine bearing samples and measured by active ultrasound. A recognition method based on one-dimensional convolutional neural network (1D CNN) is applied to identify various indentations from undamaged surfaces. Additionally, the 1D CNN model is also applied to surface damage recognition and shows a satisfactory performance, using an ultrasound in-situ measurement dataset of aluminium alloy coated samples. The result shows the 1D CNN model can effectively identify the indentations even if the ultrasound shows an undamaged indication, and it also can separate the damaged surface from the undamaged results. Generally, this technique can work as an auxiliary toolbox in an automated monitoring of journal bearing damage and make early warning in unmanned environments.

Key words: Early-state Wear, Indentation, Ultrasound Wear Measurement, One-dimensional Convolutional Neural Network, Journal Bearing Coating

1. Research background

The journal bearings are very important components in the structure of rotating machinery. However, the wear or surface damage of journal bearings is inevitable due to external impacts, overload, contamination, oil starvation, or other reasons [1], [2] . Therefore, the coating material is designed and applied as a sacrificial layer on the surface of journal bearings to wear [3]. Once the wear status exceeds the allowed threshold, there will be a lack of concentricity and rotational accuracy, leading to a temperature increase, local impact of the shaft, abnormal vibration, even severe accidents [4], [5]. Ultrasonic methods have become a popular method for detecting bearing lubrication systems in recent years, mainly focusing on measuring oil film thickness and wear depth. The ultrasonic longitudinal and shear waves have been proven to enable a micron-level wear measurement on various coating materials,

including aluminium alloy, bronze-lead alloy and Polyether ether ketone (PEEK) [6], [7]. Furthermore, signal analysis methods based on different principles, such as the resonance analysis, phase-shift analysis, and signal reconstruction, have been successively proposed, enabling more refined ultrasonic testing in the field of tribology [8], [9], [10]. Currently, a novel longitudinal-wave-based method has been reported for simultaneous measurement of lubricant film thickness and wear depth, exhibiting strong engineering adaptability and broad potential for industrial application [11]. The authors have also proposed an ultrasound-based in-situ measurement system design, which is applicable for continuous measurement of metallic journal bearing coatings, with an error within ±10 μm compared to microscopic results [12]. However, during the wear progress of bearing coating, the ultrasound results are not always accurate. Typically, it sometimes indicates a coating thickness increase when the coating surface starts to wear, although which is always followed by a continuous thickness reduction subsequently. This abnormal increase in thickness always occurs at the early stage of wear generation, and shows as a surface deformation of a wear scar with thicker edges, known as the early-state wear. This type of wear scar is usually led by the squeezing and sliding of hard asperities or particles, and the wear scar is similar with the scar of an indentation.

With the development of machine learning and neural networks, researchers have gained new insights into the characteristics of signals, which also provides new explanations for phenomena in tribology. Current research using machine learning to evaluate bearing systems mainly focuses on analyzing abnormal signals generated by structural failure, usually the acoustic emission (AE) signal. For example, the machine learning algorithms, such as Support Vector Machine (SVM) and k-Nearest Neighbour (kNN) have been applied to the AE signal classification of bearings [13], [14], [15]. However, these techniques require a prior manual analysis and feature extraction before sending these features to the classification model, which can hardly meet the requirement of real-time measurement.

Compared with traditional machine learning methods, the advantage of neural networks is that they rely on the statistical information of the samples themselves for feature extraction, without the need for prior knowledge of sample features. A CNN-based model has been reported to analyze the vibration images and Short-time Fourier Transformed (STFT) images from the vibration sensors of a rolling bearing system [16], [17]. And the Deep Neural Network has also demonstrated the ability to classify wear and fatigue in sliding bearings [18]. The Long Short-Term Memory (LSTM) algorithm allows for learning from time-series data and supports real-time monitoring by enabling direct input of the original signal or un-processed signal into the model. However, a comparative study has shown that 1D CNN models perform better than SVM and LSTM networks in classification performance [19].

1D CNN is a learning model using convolutional neural networks operating on 1D signals, usually for continuous time series, which can process data in various domains, such as time-domain, frequency-domain, and even wavelet-domain data [20], [21]. However, the existing bearing fault analysis methods based on 1D CNN only aim at vibration signals. Zhang et al. proposed a hybrid structure based on 1D CNN, residual network (ResNet), and Kolmogorov-Arnold Network (KAN) which can effectively extract deep features from bearing vibration signals under multiple operating conditions. Even under extremely limited samples and high noise levels, it can maintain an accuracy of over 90% [22]. Muratbakeev et al. constructed a 1D-CNN-LSTM model that utilizes a 1D CNN to extract local time-domain features, and then captures long-term dependencies using LSTM module, thereby improving the robustness under different conditions [23]. Wan et al. used acoustic signals instead of

contact vibration sensors, combined with wavelet packet decomposition and improved 1D CNN for fault diagnosis, proving the feasibility of non-contact acoustic signals combined with deep learning models [24]. Generally, compared with other types of machine learning methods, 1D CNN can automatically extract features from raw data in signal classification tasks, which enables them to classify unknown signals more quickly in practical applications [25]. Table 1 shows some representative researches on 1D signals above, which shows a high accuracy on the classification of 1D signals and can be further improved combing with other methods.

Table 1. Representative researches on 1D signal classification.

Ref.	***Year***	***Data Type***	***Test Objects***	***Algorithm***	***Accuracy***
[25]	*2017*	*Vibration Signal*	*Ball bearing, fault or not*	*1D CNN*	*97.1%*
[13]	*2021*	*Vibration Signal*	*Roller bearing, fault position*	*SVM*	*85.36%*
[18]	*2021*	*AE Signal*	*Slide bearing, wear mode*	*DNN*	*82.5%*
			Slide bearing, fatigue mode		*98.7%*
[14]	*2022*	*AE Signal*	*Roller bearing, fault position*	*SVM*	*97.13%*
			Roller bearing, fault size		*96.9%*
[19]	*2025*	*Vibration Signal*	*Ball Bearing (fault mode)*	*1D CNN*	*99.83%*
				LSTM	*98.7%*
				SVM	*97.8%*
[22]	*2025*	*Vibration Signal*	*Roller bearing, fault mode*	*Hybrid*	*100%*
[24]	*2025*	*Vibration Signal*	*Roller bearing, fault position*	*1D CNN*	*100%*

In this study, active ultrasound was used to measure the wear of bearing shells, which provides a more accurate understanding of their surface condition compared to previous vibration-based methods. Additionally, unlike LSTM, which can also process time-series data, 1D CNN is generally more computationally efficient and quicker to train, which are essential for real-time signal classification applications where both speed and accuracy should be considered, especially during the rotation. Therefore, the 1D CNN structure is finally selected in this research to achieve the recognition of the early-state wear.

In this article, the formation of early-state wear and the ultrasound behaviour at the early wear state will be initially investigated, through the theoretical study and finite-element analysis. Then, the early-state wear scar is simulated by the indentation process, and the active ultrasound and a machine learning model based on 1D CNN are proposed to recognize the material deformation and subsequent wear of bearing coatings. This article innovatively proposes a method for identifying early-state wear, which can effectively identify the abnormal state of the coating before the material loss, usually in the deformation stage. This

method will also make a significant contribution to the health monitoring of important rotating machineries or unmanned devices in the future.

2. Wear mechanism of journal bearing coatings

2.1 Typical wear types of journal bearing coatings

Regarding the surface damage of sliding bearings, research shows that over 80% of bearing failure has been led by the wears, especially the abrasive wear (59.4%) and adhesive wear (18.9%) [26]. Abrasive wear usually generates when a hard material slides against a softer material, resulting in the removal of material from the softer surface [27]. And it is always shown as long parallel grooves, mild scratches, or severe gouging along the sliding direction. For the adhesive wear, it is usually shown as a soft material removal adhering to the surface asperities of a more rigid surface [28]. The principle of abrasive wear and adhesive wear are shown by Figure 1.

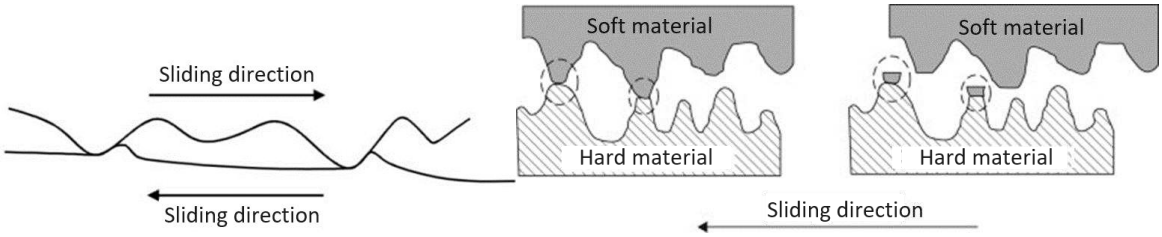

(a) (b)

Figure 1. The diagram of (a)Two-body abrasive wear, and (b)Adhesive wear.

However, during the operation of journal bearings, the wear mechanisms and the wear scars are always complicated. Figure 2 shows two cross-sectional images in circumferential directions from previous experiments (cut along the axial direction), the in-situ measurement of aluminium-alloy coated journal bearing shells. Figure 2(a) shows a deep groove shaped scar, with thicker material on both sides of the groove. Figure 2(b) shows a more common cross-section of wear, with a series of small and discontinuous scratches along axial direction.

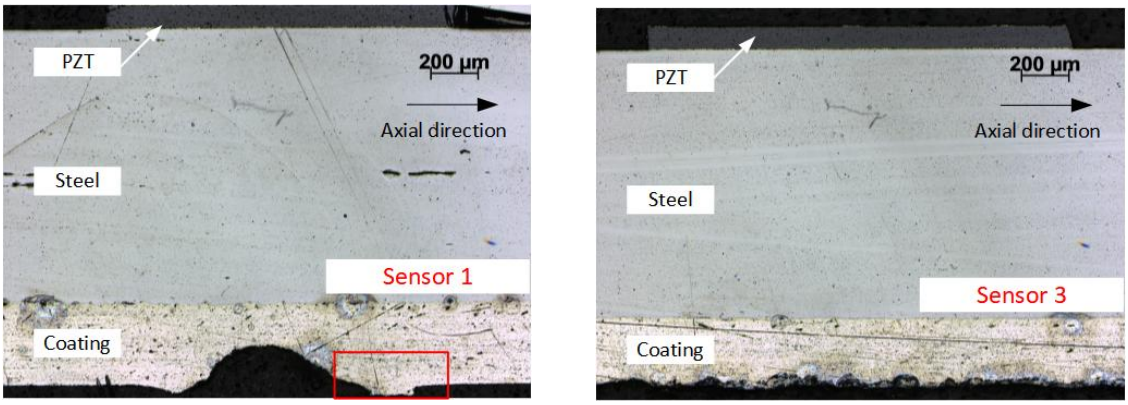

(a) (b)

Figure 2. The cross-section image of a damaged aluminum-alloy coated bearing shell. (a)A deep groove shaped wear scar, and (b)A common worn surface.

In fact, the wear scar shown in Figure 2(a) was accidentally observed during a dry-contact experiment, which was not common in a long-term running. This is because during a

long-term operation, the thicker coating area will be subsequently removed due to a continuous friction, as the region shown in the red column in Figure 2(a). It shows a flat but thicker surface in the red column, which means some material has been removed.

2.2 The mechanism during coating wear progress

Based on Figures 1 and 2, a wear mechanism of bearing coatings under actual operation can be proposed, as shown in Figure 3(a). At the early stage of wear, due to the contact and friction, the surface of softer coating materials is compressed by harder particles or surfaces, forming local deformation of the material. At this stage, abrasive wear is the dominant wear type, with a small amount of material removed, but thicker areas formed. Afterwards, because of friction, the material in thicker areas is removed. At this stage, both abrasive and adhesive wear generate simultaneously. For a long-term operation, these two stages work alternatively, and finally forming a large area of material loss. But in the continuous ultrasound measurement, the previous result shows an increasing first and then decreasing trend of coating thickness, as an example shown in Figure 3(b).

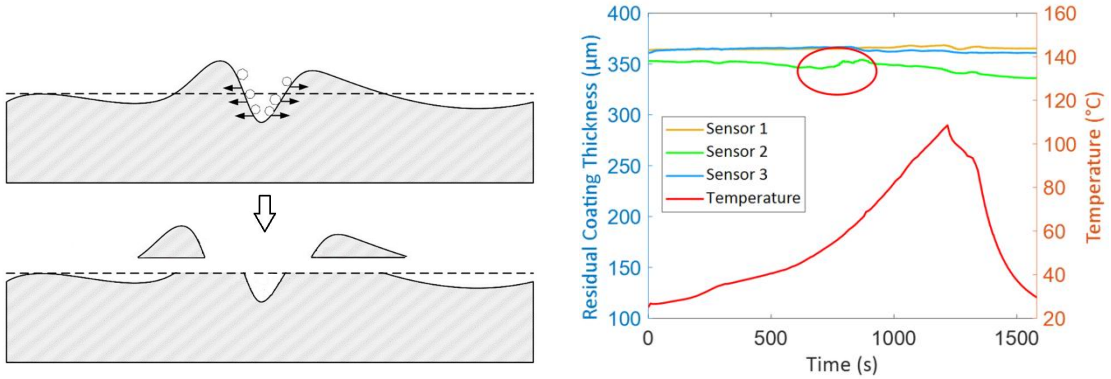

(a) (b)

Figure 3. (a)The diagram of wear progress of journal bearing coating. (b)An example of the continuous wear progress measured by active ultrasound.

According to the proposed mechanism, the wear of journal bearing coating begins with the deformation of the material, which has a similar profile with the indentation. And at this stage, it can be considered that there is no substantial material removal. In this case, ultrasound testing will display an inaccurate coating thickness, which is often greater than its actual thickness. Although this process may occur briefly during long-term testing, its periodic occurrence may temporarily lead to a wrong estimate of the coating thickness and wear level. Therefore, if there is a method that can identify the signals of indentation and early-state wears, it will enhance the credibility of ultrasound in a long-term monitoring.

3. Ultrasound behaviour and measurement of indented surfaces

3.1 Creating indentation on coated bearing samples

To simulate the scar of the early-state wears, some indentations were created using a loading machine. The depth of the indentations is between 60μm and 120 μm, slightly shallower than the deformation caused by dry contact in Figure 2(a). The diagram of loading process is shown in Figure 4(a). Five bronze-lead (Cu-Pb) coated marine bearing samples were processed with indentations and the coating of each sample was processed with three

different loads, 50 N, 100 N and 150 N, as shown in Figure 4(b). The length of the indentation is 10 mm, and the spacing between adjacent indentations is 8 mm. An example of the profile of the indented surface (Sample 1) is shown in Figures 4(c).

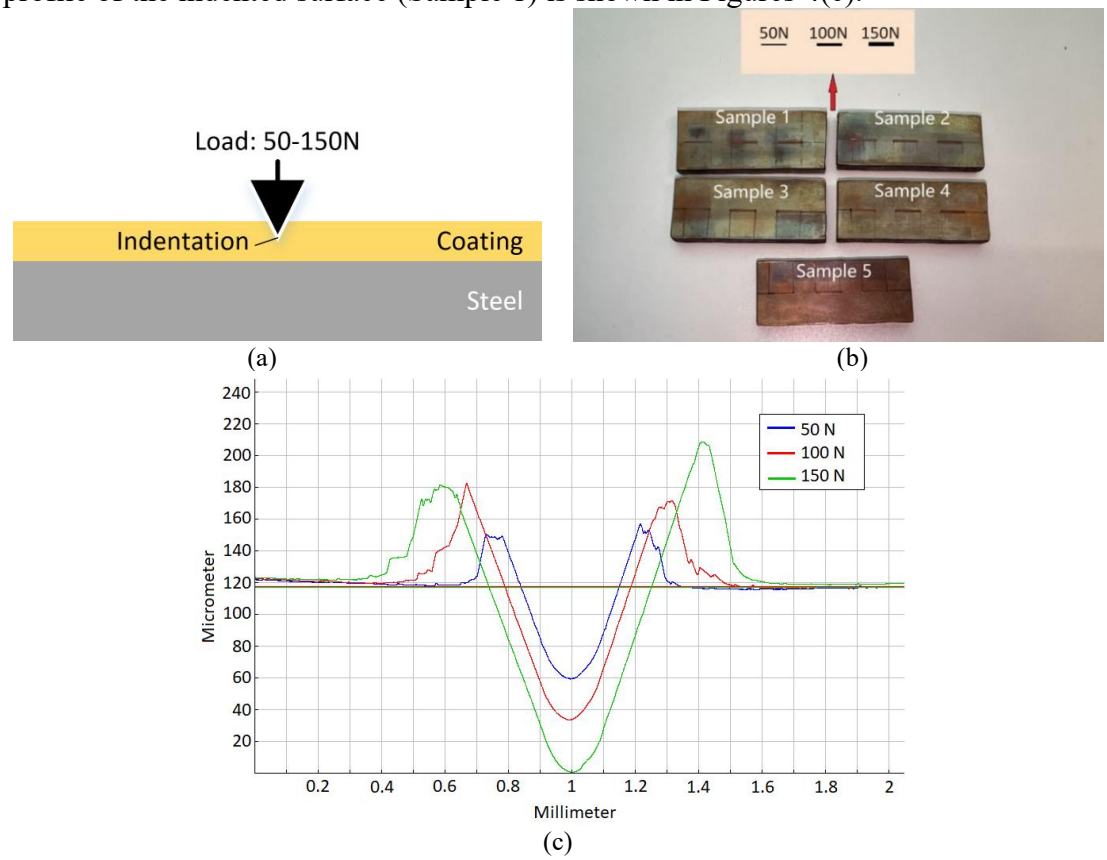

Figure 4. (a)The indenting process of bronze-lead coated bearing sample. (b)Bearing samples with indented surface. (c)An example of the indentation profile of Sample 1.

3.2 The interaction between the ultrasound and indentation

In order to study the ultrasound behaviour at the indented coating surface before actual testing, a copper-steel double layered structure was modelled to simulate a small area of an indented bearing coating using a finite element software COMSOL Multiphysics. It is worth mentioning that in numerical modelling, pure copper was chosen as the coating material because of its similar acoustic properties to Cu-Pb alloy. The reflection of ultrasound at the copper-steel interface is also similar to the reflection pattern at steel and Cu-Pb alloy interfaces. The 22 MHz signal was used as the input frequency and the material properties in the simulations are shown in Table 2.

Table 2. Properties of materials in finite element modelling.

Description	***Density (g/cm^3)***	***Thickness (mm)***	***Width (mm)***	***Young's modulus (10^9 Pa)***	***Poisson's ratio***
Copper Coating Layer	*8.96*	*0.5*	*4*	*110*	*0.35*
Steel Bearing Layer	*7.85*	*4.5*	*4*	*205*	*0.28*

A zero displacement and zero velocity were set as initial conditions and the sound pressure at all the outer edges were set to zero. The governing equation of elastic wave is expressed as:

$$\frac{E}{2(1+\nu)}[\nabla^2\mathbf{u}+\frac{1}{(1-2\nu)}\nabla(\nabla\cdot\mathbf{u})]+\mathbf{F}=\rho\frac{\partial^2\mathbf{u}}{\partial t^2} \quad (1)$$

In Equation 1, E represents the Young's modulus, ν represents Poisson's ratio and ρ is the density of media. The displacement and boundary pressure are in vector form, $\mathbf{u}$ and $\mathbf{F}$.

Figure 5(a) shows an example of the simulation of an indentation scar, which is similar with the dimension of the 150 N loaded indentation in Figure 4(c). The two edges are set as the same size to simplify the model set-up. The blue line in Figure 5(a) represents the ultrasound input and receiving area (2mm), which is also equal to the length of practical ultrasound sensor. The ultrasound input direction is perpendicular to the top surface. The amplitude of ultrasound input is expressed as:

$$|\mathbf{F}|=[1-\cos(\frac{2\pi ft}{3})]\cdot\sin(2\pi ft) \quad (2)$$

The notation PML in Figure 5(a) stands for a perfect matched layer, which is used to absorb the reflected waves. The time step is in the range $t\in[0,3/f]$, where f is the ultrasound input frequency, set as 22 MHz, equal to the ultrasound frequency used in actual tests. The grid size of meshing was set between 10μm and 50μm. It was 50μm at some remote or regular-shaped area and 10μm at the discontinuous region, such as a corner or damage. The models were built to simulate the indentations in Figure 4(c) accordingly, to investigate the reflection from the indented coating surface. The results are shown as Figure 5(b).

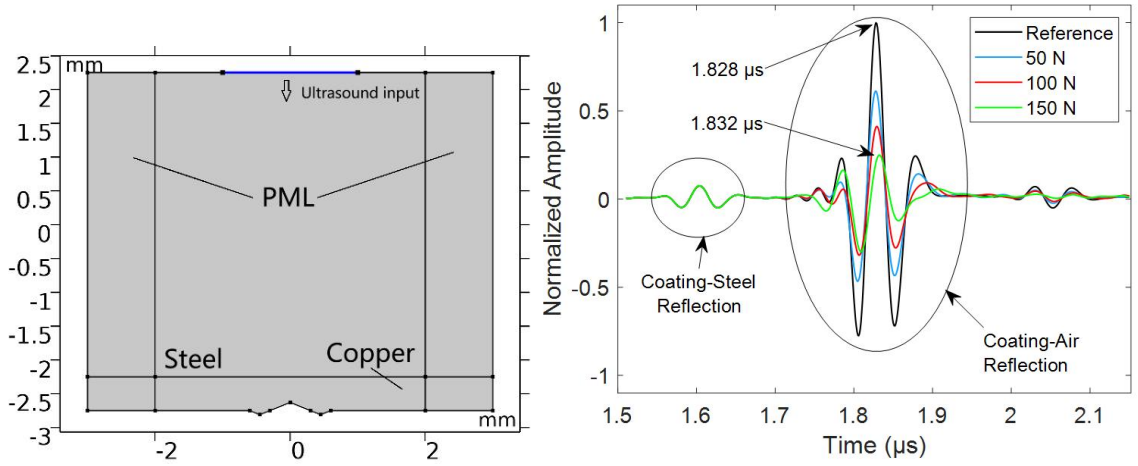

(a) (b)

Figure 5. (a)Diagram of the 150 N loaded indentation scar; (b)Simulation result of ultrasound reflections from different indentation scars.

In Figure 5(b), the black curve represents the reference signal; that is the reflection from an undamaged surface. The blue, red and green curves are corresponded to the 50 N, 100 N and 150 N loaded conditions, which are in the same color with the legends in Figure 4(c). In Figure 5(b), the reflections from the copper-steel interface and copper-air interface can be observed. All the data has been normalized and the amplitude of coating-steel reflections are the same, which means there is no damage to the coating-steel interface. For the coating-air interface, when the indentation is larger, the ultrasound reflection shrinks a lot. Specifically, when the indentation is larger, as marked in Figure 5(b), the peak of the reflection pulse could

shift rightwards. When using the Time-of-Flight method to calculate the coating thickness, it could lead to a longer ToF, subsequentially a larger measured thickness value.

The shift of ultrasound reflection at the indentation is further investigated by observing the ultrasound reflection in the numerical model. The ultrasound reflection at the 50 N and 150 N indentations are shown in Figure 6.

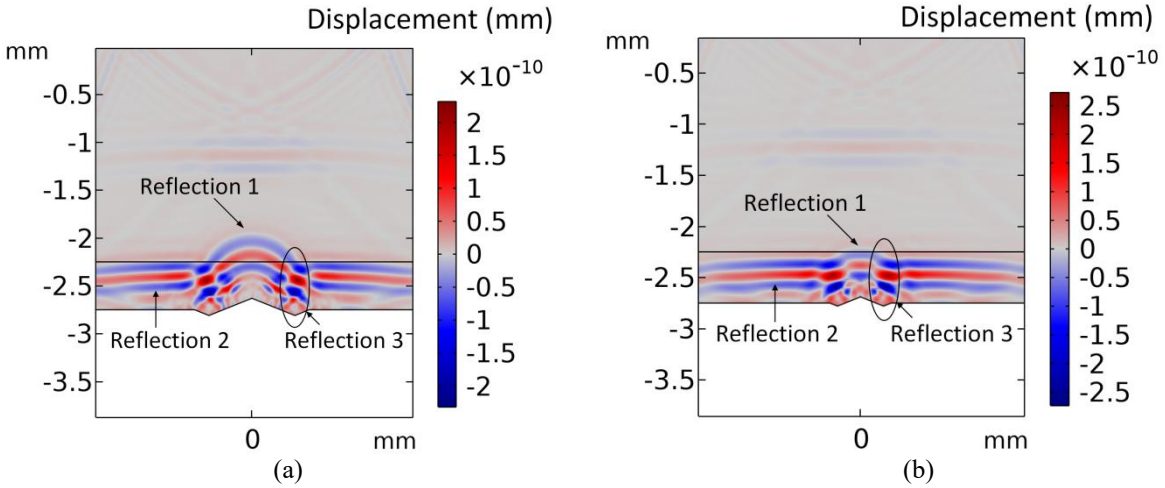

Figure 6. The wavefront of ultrasound reflection from the indentation, (a) 150 N loaded; and (b) 50 N loaded.

The overall reflection from the 150 N indentation consists of three reflections, the reflection from the middle of indentation (Reflection 1), the undamaged surface (Reflection 2) and the edges (Reflection 3), as shown in Figure 6(a). Due to the deformation of material, the Reflection 1 reflects back earlier than the other two reflections. At the same time, due to the shape of the indentation, a portion of the ultrasound energy is scattered to both sides. Therefore, the wavefront of Reflection 1 shows as a curved front.

In addition, under the influence of shape, ultrasound focuses on the edge of the indentation, which results in more energy being concentrated by the reflection at the edge of indentation. This can be inferred from the color in Figure 6(a), where the color of Reflection 3 is noticeably darker. After the superposed signal of Reflection 3 and Reflection 2 is received by the sensor, this reflection shows a delayed time of arrival. This reveals why ultrasound sometimes reports an increase in thickness when detecting early deformation of materials.

In contrast, the wavefront reflected by the indentation under a 50 N load is more similar to a plane wave, as shown in Figure 6(b). In this case, a small amount of energy is scattered to both sides, so the amplitude shrinkage of the blue curve in Figure 5(b) is smaller and much closer to the black reference signal. However, this also means that subtle deformations are difficult to distinguish. Therefore, in actual testing, for early deformation of material surface (similar in shape to indentation), ultrasound is difficult to obtain an accurate result of deformation. This requires a method to determine whether the material has deformed or not during the monitoring, based on real-time ultrasound signals.

3.3 Ultrasound measurement of indentations

Based on the analysis in Section 3.2, the ultrasound measurement was carried out using the samples in Section 3.1, to investigate the ultrasound behaviour at the indentation. The 22

MHz ultrasound sensors were mounted along the direction of the indentation on the other side of the bearing samples and covered the entire indentation. And some extra sensors were mounted onto the undamaged area to obtain the speed of sound, about 3933.80 m/s under the room temperature (~20°C). However, because of the curved surface profile of the indentation, the reflection from the indented surface was complicated, which could be regarded as a superposition of the reflections from different surface level, as described in Figure 6.

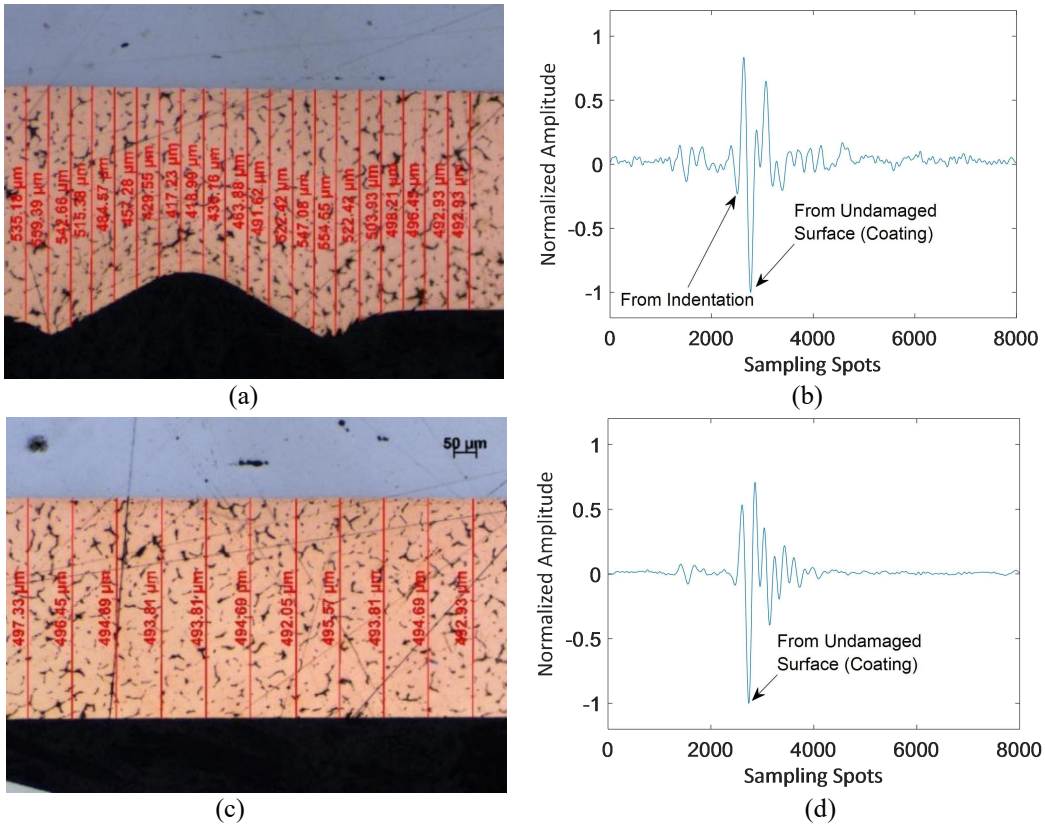

Figure 7. An example of the cross-section view of the indentation and received signal of Sample 1. (a)Cross-section of the indentation under 100 N load, (b)The first reflection of Figure 7a, (c)Cross-section of an undamaged area, and (d)The first reflection of Figure 7c.

Figure 7(a) shows the indented surface of the area under Sample 1, created by 100 N load. Figure 7(b) shows the reflected signal from that surface. For a better comparison, Figure 7(c) and 7(d) depict the surface and the reflected signal from the undamaged area of Sample 1, a sensor used for speed of sound calibration.

Comparing the waveforms in Figure 7(b) and 7(d), when there is an indentation under the sensor covered area, the reflected signal at the coating-air interface becomes more complex and shows as a superposition of two reflected signals from different levels. One of them represents the reflection from the thinnest location of indentation and the other represents the reflection from the average level of the coating surface. Therefore, based on the amplitude change of the reflected signal, the signal from the indentation and the average level of the surface can be separated, as the tips shown in Figure 7(b).

3.4 Result of indentation measurements

For the indentation measurement, the coating thickness at the indented location (minimum thickness of the coating) and the average thickness of the coating under the sensor have been

calculated using the ToF of two separated reflection signals. The comparison between ultrasound result and microscope result are in Tables 3. In Tables 3, the results of the minimum thickness test of some sensors left blank, because the reflected signals in the minimum thickness area were difficult to separate out. For the five bearing samples, the greater the load was during the indentation process, the deeper the indentation depth, and more obvious separated reflections could be observed.

Table 3. (a)The indentation measurement of bearing Sample 1.

		Test 1	*Test 2*	*Test 3*
Applied Load (N)		*50*	*100*	*150*
Average Thickness (μm)	*Ultrasound*	*480.79*	*499.94*	*531.01*
	Microscope	*461.91*	*494.42*	*541.03*
	Deviation	*18.88*	*5.52*	*10.02*
Minimum Thickness (μm)	*Ultrasound*	*-*	*397.25*	*412.16*
	Microscope	*-*	*417.23*	*444.08*
	Deviation	*-*	*19.98*	*31.92*
Depth of Indentation (μm)	*Ultrasound*	*-*	*97.17*	*128.87*
	Profile Meter	*58*	*85*	*120*

Table 3. (b)The indentation measurement of bearing Sample 2.

		Test 1	*Test 2*	*Test 3*
Applied Load (N)		*50*	*100*	*150*
Average Thickness (μm)	*Ultrasound*	*532.73*	*530.04*	*460.95*
	Microscope	*555.32*	*501.49*	*437.44*
	Deviation	*22.59*	*28.54*	*23.51*
Minimum Thickness (μm)	*Ultrasound*	*-*	*428.62*	*346.96*
	Microscope	*-*	*422.08*	*344.61*
	Deviation	*-*	*6.54*	*2.35*
Depth of Indentation (μm)	*Ultrasound*	*-*	*101.42*	*114.00*
	Profile Meter	*60*	*95*	*110*

Table 3. (c)The indentation measurement of bearing Sample 3.

		Test 1	*Test 2*	*Test 3*
Applied Load (N)		*50*	*100*	*150*
Average Thickness (μm)	*Ultrasound*	*470.49*	*536.70*	*542.59*
	Microscope	*495.15*	*502.95*	*550.76*
	Deviation	*24.66*	*33.74*	*8.17*
Minimum Thickness (μm)	*Ultrasound*	*-*	*-*	*435.57*
	Microscope	*-*	*-*	*455.08*
	Deviation	*-*	*-*	*19.51*
Depth of Indentation (μm)	*Ultrasound*	*-*	*-*	*107.02*
	Profile Meter	*50*	*95*	*113*

Table 3. (d)The indentation measurement of bearing Sample 4.

		Test 1	*Test 2*	*Test 3*
Applied Load (N)		*50*	*100*	*150*
Average Thickness (μm)	*Ultrasound*	*468.22*	*545.79*	*547.59*
	Microscope	*479.06*	*527.72*	*545.16*

	Deviation	*10.83*	*18.07*	*2.43*
Minimum Thickness (μm)	*Ultrasound*	*-*	*442.71*	*445.79*
	Microscope	*-*	*444.96*	*454.64*
	Deviation	*-*	*2.25*	*8.85*
Depth of Indentation (μm)	*Ultrasound*	*-*	*103.08*	*101.80*
	Profile Meter	*53*	*95*	*115*

Table 3. (e)The indentation measurement of bearing Sample 5.

		Test 1	*Test 2*	*Test 3*
Applied Load (N)		*50*	*100*	*150*
Average Thickness (μm)	*Ultrasound*	*464.01*	*513.71*	*540.65*
	Microscope	*448.48*	*503.58*	*548.47*
	Deviation	*15.53*	*10.13*	*7.82*
Minimum Thickness (μm)	*Ultrasound*	*-*	*-*	*425.50*
	Microscope	*-*	*-*	*454.20*
	Deviation	*-*	*-*	*28.70*
Depth of Indentation (μm)	*Ultrasound*	*-*	*-*	*115.15*
	Profile Meter	*53*	*90*	*118*

Generally, for all of the five samples, it is hardly to detect indentations of around 50 μm created by the 50 N load, which is similar to the simulation results in Section 3.2. Part of the indentations created by 100 N load can be detected, while the indentations created by 150 N load can be fully detected. For the situation where indentation is detected, the deviation between the indentation depth measured by ultrasound and the profile meter is basically within 10 μm, except Sample 1 Test 2, about 12.17 μm.

However, during the ultrasound in-situ measurement, the average thickness is used to determine the wear condition of the coating material. According to the results in Table 3, there is a maximum deviation of 33.74 μm (Sample 3, Test 2), which is caused by the irregular shape of the indentation. This deviation could lead to an incorrect interpretation of the residual thickness. Therefore, it will be helpful if there is an auxiliary method to cooperate with the ultrasound, to determine if there is an early-state damage (indentation shaped damage).

4. Bearing shell wear recognition using 1D CNN

4.1 Principle of 1D CNN

An ultrasound signal is essentially a numerical sequence and the extraction of features is always required when identifying the abnormal conditions, for example, the indentation or wear on the coating surface. The time-frequency analysis tools, such as STFT and wavelet, are often used to extract these local features of signals, as the marked tips in Figure 7(b). These methods generally use a set of manually defined functions, also known as basis, to extract local features of the signal by shifting or scaling along the sequence.

Different from the above tools, in the 1D CNN model, multiple convolutional kernels are trained to extract different local features. For example, in Figure 8, w_1, w_2, w_3 is a convolution kernel of length 3, while a_1, a_2, ... a_n is the ultrasound sequence of length n. Each

convolution kernel slides on the ultrasound sequence, calculates the local dot product c_{11}, c_{12}, … c_{1n}, and biases it (bias term not specified in Figure 8). At this point, c_{11}, c_{12}, ... c_n in the convolutional layer represents the similarity between the convolutional kernel and the sequence, known as feature extraction. The process of convolution kernels sliding on a sequence is similar to the translation and scaling in wavelet transform. These kernels can be regarded as an independent weight vector, which will be further trained in the 1D CNN model, usually set through the number of output channels of convolutional layers [29].

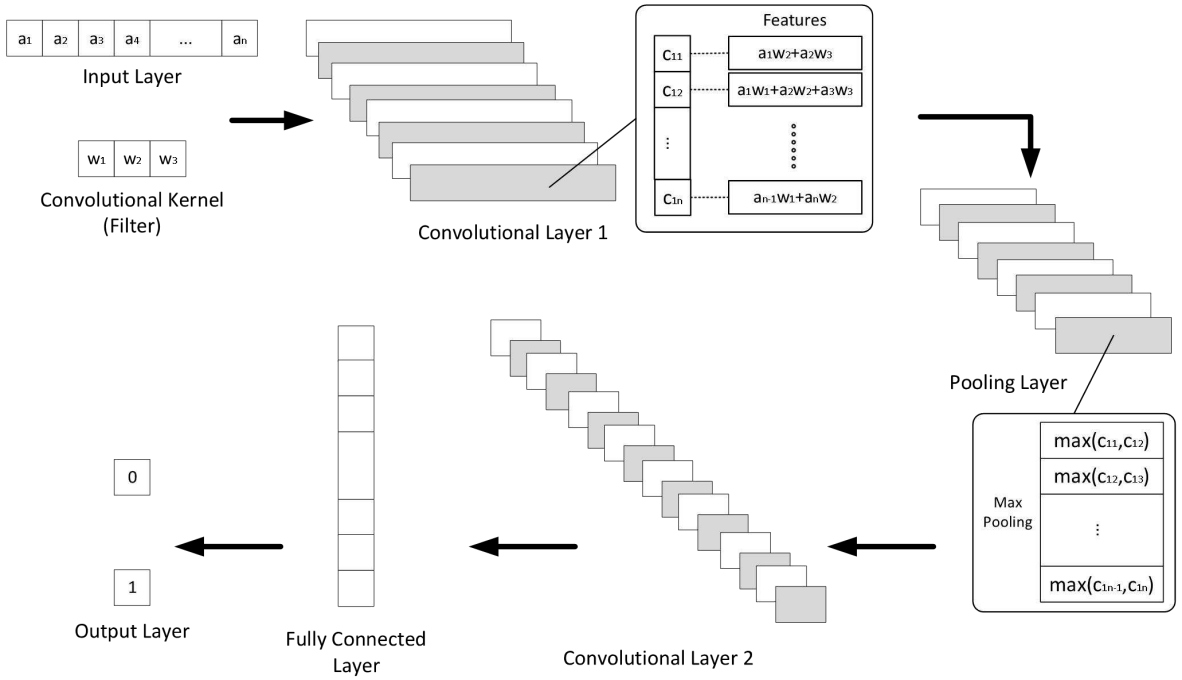

Figure 8. The diagram and dataflow of 1D CNN (bias not specified).

Then, the Pooling operation has been utilized to compress the dataflow while keeping the previous features after convolution. In the model of this article, the length of the Pooling Kernel is 2, and the maximum pooling method is operated, which takes the maximum value of adjacent elements for output, e.g., $\max(c_{11}, c_{12})$, retaining the most significant features of the original signal [30]. The data output of the Pooling Layer is unfolded into a 1D vector after an extra feature extraction, forming a Fully Connected Layer (FC Layer). At this point, each element (neuron) of the FC Layer is connected to all neurons in the previous layers. Based on the deviation between the FC Layer and the real value of input data (known as Label), the weight of the neurons (w_1, w_2, w_3) is self-adjusted to minimize the overall loss. The Cross Entropy Loss Function is defined as the loss function of the model, and the Adaptive Moment Estimation algorithm (Adam) is used to update the weights and biases of the model. The Cross Entropy Loss Function is given by:

$$Loss = \frac{1}{N}\sum_{i} -[y_i \cdot \log(p_i) + (1-y_i)\cdot \log(1-p_i)] \tag{3}$$

Where y_i is the label of sample i and p_i is the probability of sample i being predicted as positive. For example, during the training process, when determining whether a sample y comes from a damaged surface, it is assumed that the label of the undamaged interface is 1 (positive) and the label of the damaged surface is 0. When the sample indeed comes from an undamaged interface and the predicted value is p, the loss value is -log(p). In this way, when

the predicted value p of the model differs greatly from its true value, the loss of the sample point will be extremely high, and vice versa.

The activation function has been employed to enhance the model's capacity to address non-linear problems and to determine the activation status of neurons in subsequent layers. In this research, the Rectified Linear Unit (ReLU) function is utilized to process the output of convolutional layers to avoid overfitting. The model properties are shown in Table 4. The hardware configuration used in this article is AMD Ryzen 9 5900HX (8 cores, 12 threads, 3.30GHz CPU), 32GB DDR4 3200MHz RAM, 1TB NVMe SSD for dataset storage, and PyTorch 2.2.1 framework.

Table 4. The description of 1D CNN model properties.

Model Properties	***Description***
Convolutional Layer 1 (Conv1)	*Kernel size / Stride / Padding = 3 / 1 / 1*
Convolutional Layer 2 (Conv2)	*Kernel size / Stride / Padding = 3 / 1 / 1*
Pooling Layer	*Kernel size / Stride / Padding = 2 / 2 / 0*
Pooling Operation	*Max Pooling*
Loss Function	*Cross Entropy Loss*
Activation Function (before Pooling Layers)	*ReLU*
Activation Function (before FC Layer)	*Softmax*
Optimizer	*Adam Algorithm (learning rate = 0.0001)*

In general, the advantage of using 1D CNN to analyze indentation signals is that 1D CNN can automatically capture local features of indentation signals. This means that for the echo signals reflected by different indentations, they always have some commonalities, such as a tip in the main echo in Figure 7 (b), which may correspond to a certain feature in 1D CNN. The final trained convolution kernel represents the feature information of certain parts of the raw ultrasound signal, which may contain some high-dimensional features as well. But due to the differences in materials, the specific details of the model, including parameters such as features and weights, are potentially in different values.

4.2 The indentation recognition using 1D CNN

In Table 3, when using ultrasound to measure the average thickness, it shows a large deviation which was not consistent with the actual damage and could result in an underestimate of the actual damage. Moreover, for some indented groups under 50 N and 100 N load, ultrasound is also difficult to give an accurate result. Therefore, in this section, an indentation recognition model will be established and used to determine whether there is an indentation-shaped damage on the surface. To enhance the generation performance of the 1D CNN model, all signals have been normalized and their amplitudes have been normalized between $[-1,1]$. Moreover, the data are randomly trimmed to reduce the correlation between groups and improve the model's generalization ability, as an example in Figure 9.

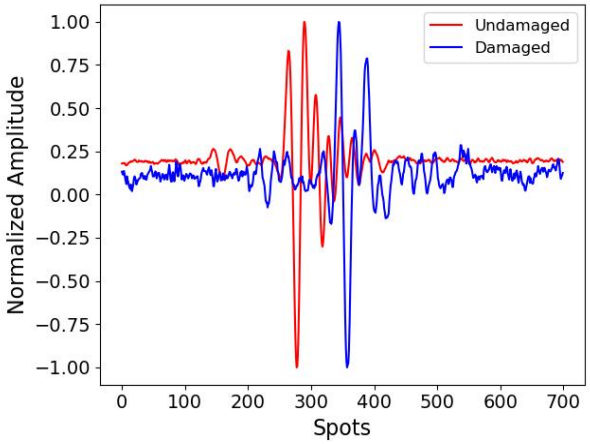

Figure 9. The randomly trimmed and normalized signals of the undamaged and damaged surface.

The data set division is shown in Table 5(a), which has been divided into training, validation and test set, with a proportion of 6:2:2. Specifically, 60% of the data was used for training, as the training set in Table 5(a), while 20% was used to calculate the loss during each epoch, as the validation set. The rest 20% was divided as the test set, to get the classification accuracy. It is worth noting here that the data in test set is not used for model training.

The initial number of training epochs was set as 500, with an early stopping patience 5 and 10. That is, if the validation loss no longer decreases after several consecutive 5 or 10 epochs, the training will be terminated, and set the current model parameters as the wanted ones.

After each epoch, the test accuracy was calculated and finally plotted in Figure 10. To find the optimized parameters of the 1D CNN model, various combinations of the model parameters were used to build the classifier. The structure complexity has been compared and results are shown in Table 5(b).

Table 5. (a)The description of sample size and labels (indentation recognition models).

	Train Set Size	*Validation Set Size*	*Test Set Size*	*Label*
Undamaged	*540*	*180*	*180*	*1*
Damaged	*900*	*300*	*300*	*0*

Table 5. (b)The comparison of structure complexity of indentation recognition models.

Number of Convolutional Layers	*Number of features (kernels per layer)*	*Number of FC layers*	*Accuracy*	
			Patience = 5	*Patience = 10*
1	*2*	*1*	*84.17%*	*83.75%*
1	*4*	*1*	*93.96%*	*95.42%*
1	*8*	*1*	*93.33%*	*93.96%*
1	*16*	*1*	*93.12%*	*93.75%*
2	*2/4*	*1*	*90.21%*	*90.00%*
2	*4/8*	*1*	*98.33%*	*98.54%*
2	*4/16*	*1*	*98.75%*	*98.54%*
2	*2/4*	*2*	*96.67%*	*96.67%*
2	*4/8*	*2*	*98.96%*	*98.96%*
2	*4/16*	*2*	*98.12%*	*97.92%*

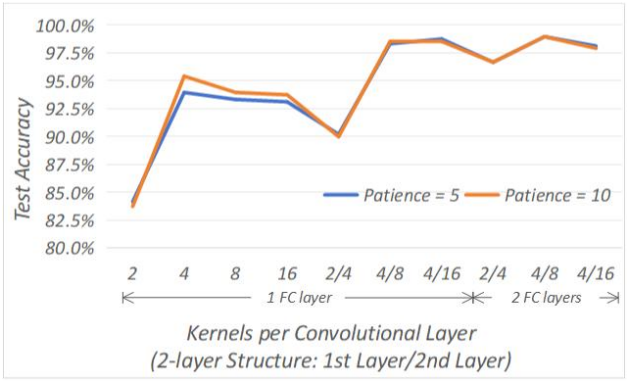

Figure 10. The comparison of structure complexity of indentation recognition models.

According to the results in Tables 5(b), as the model complexity increases, the accuracy of classification tasks gradually increases. When the patience value is higher, there is less influence to the classification accuracy. The classifier performs best when there are four features of the first convolutional layer output. Then, as the number convolutional layer or the FC layer increases, it shows a better result compared to the single convolutional layer structure. When there are four kernels and eight kernels in the first and second convolutional layer, and two FC layers, the classification accuracy is the highest, about 98.96% when patience=10. Figure 11 shows two examples of the training results when patience = 10.

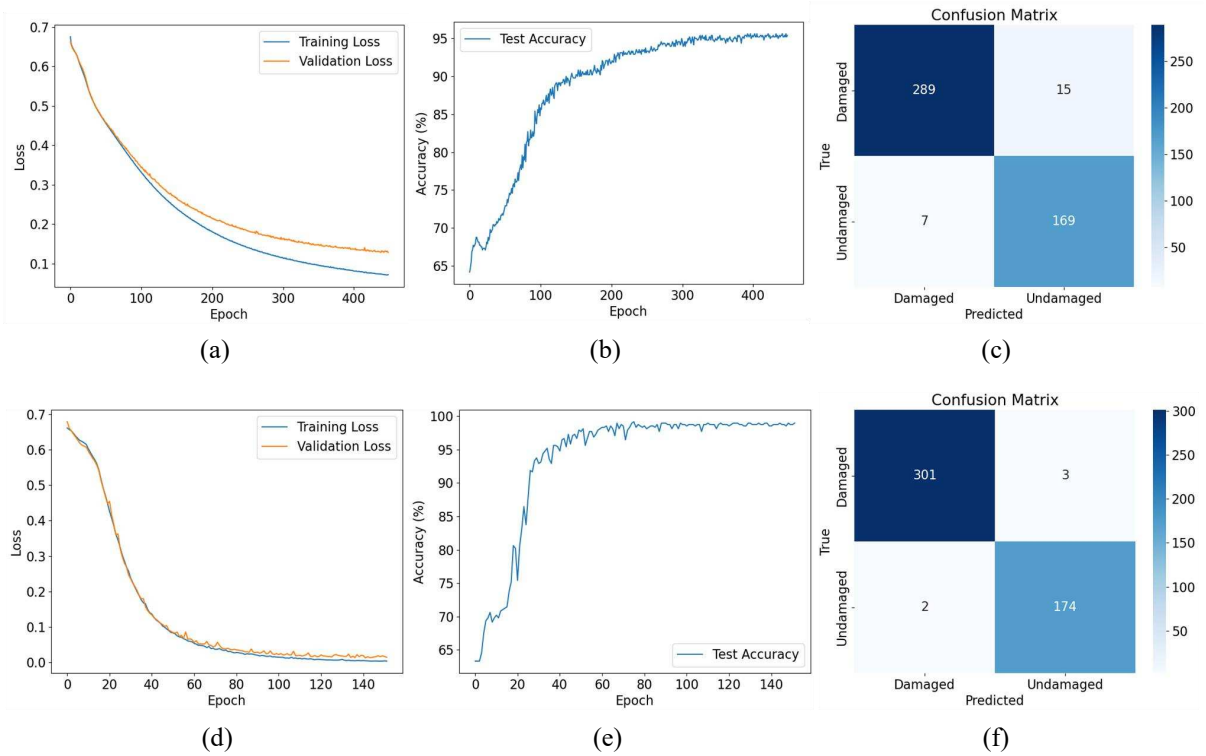

Figure 11. The change of loss values and test accuracy during the indentation recognition training, and the confusion matrix of the trained model (patience = 10). One convolutional layer, four convolution kernels, one FC layer, (a)loss changes, (b)test accuracy and (c)confusion matrix. Two convolutional layers, 4/8 convolution kernels, two FC layers, (d)loss changes, (e)test accuracy and (f)confusion matrix.

According to Figures 11, 1D CNN can effectively identify the indentations. Concerning the predicted results in Figure 11(c) and (f), both of the models show a high classification accuracy. In Figure 11(c) and (f), there are still some samples with indentation have been

classified as undamaged samples, but better than the performance of using ultrasound signal only. Moreover, the losses in Figures 11(a) and (d) show a trend of continuous convergence. During the training process of the indentation recognition model, the accuracy of the model on the validation set continued to increase, but there were fluctuations in the early stage of the process, which may be affected by parameter adjustments during the model training.

4.3 The wear recognition using 1D CNN

In this section, the classifiers based on 1D CNN are used for the classification of general bearing surface damage and on a different coating material. The data is from the aluminum-alloy coated testing samples, including artificial damages, dry-running and in-situ tests. Therefore, the training and validation set contain all the type of surface damages, including the cases similar with Figure 2(a). The signals were also trimmed and normalized to enhance the generalization ability. The initial number of training epochs was 500, with an early stopping break. The division of the dataset was followed the same proportion with the division in Section 4.2, as shown in Table 6(a) and results are shown in Table 6(b).

Table 6. (a)The description of sample size and labels (wear recognition models).

	Train Set Size	*Validation Set Size*	*Test Set Size*	*Label*
Undamaged	*3096*	*1032*	*1032*	*1*
Damaged	*3816*	*1272*	*1272*	*0*

Table 6. (b)The comparison of structure complexity of wear recognition models.

Number of Convolutional Layers	*Number of features (kernels per layer)*	*Number of FC layers*	*Accuracy*	
			Patience = 5	*Patience = 10*
1	*2*	*1*	*83.33%*	*84.90%*
1	*4*	*1*	*89.76%*	*90.49%*
1	*8*	*1*	*93.32%*	*95.44%*
1	*16*	*1*	*95.88%*	*97.92%*
2	*2/4*	*1*	*87.46%*	*88.63%*
2	*4/8*	*1*	*97.35%*	*98.05%*
2	*4/16*	*1*	*98.22%*	*98.78%*
2	*2/4*	*2*	*99.78%*	*99.74%*
2	*4/8*	*2*	*99.78%*	*99.87%*
2	*4/16*	*2*	*99.78%*	*99.83%*

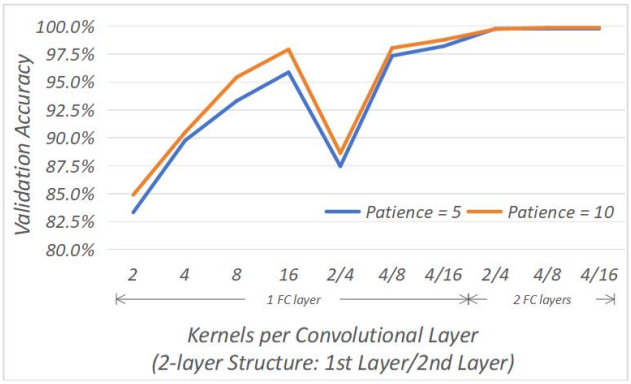

Figure 12. The comparison of structure complexity of wear recognition models.

In Table 6(b), the simplest model structure can finish the classification target with the accuracy of 84.90% (patience=10). When there are more output features (convolution kernels), the accuracy goes higher. Unlike the structure of the indentation recognition model, in the wear recognition, a single-convolutional-layer model with 16 kernels performed better, with the accuracy of 97.92%. Due to the diversity of wear surfaces, the number of convolution kernels, as well as the features, have been increased.

When the structure is more complicated, which means more convolutional layers or FC layers, the accuracy can still be enhanced. However, overfitting may occur when the structure is complicated, usually manifested as a decrease in training loss and an increase in validation loss within a few epochs. Figure 13 shows two examples of the training results (patience = 10), which Figure 13(a)-(c) correspond to a simple structure and Figure 13(d)-(f) correspond to a complicated structure.

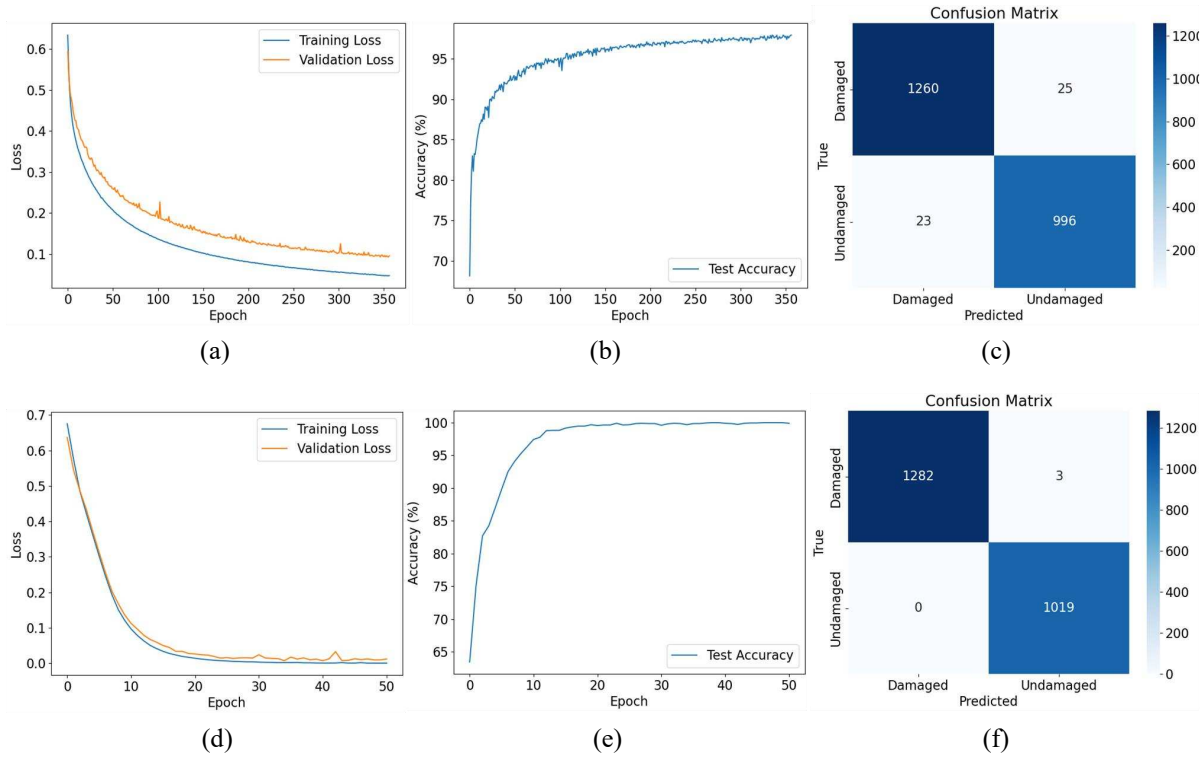

Figure 13. The change of loss values and test accuracy during the wear recognition training, and the confusion matrix of the trained model (patience = 10). One convolutional layer, 16 convolution kernels, one FC layer, (a)loss changes, (b)test accuracy and (c)confusion matrix. Two convolutional layers, 4/8 convolution kernels, two FC layers, (d)loss changes, (e)test accuracy and (f)confusion matrix.

According to the results in Figures 13(a) and 13(d), both the training loss and validation loss show a convergence trend, which means the losses continue to decrease during the training process and there is no over-fitting during the training process. And the classification model can effectively distinguish whether there is damage on the surface. Furthermore, as shown in Figures 13(b) and 13(e), as the number of epochs increases, the accuracy of classification first rapidly increases and then gradually stabilizes. In Figure 13(c) and (f), few damaged samples have been classified as undamaged samples, when there are two convolutional layers (four and eight kernels per layer) and two FC layers, only three damaged samples have been classified into the incorrect categories.

The results in Table 6 show that increasing the patience value slightly improves the classification accuracy of models with equivalent complexity, suggesting that the models may benefit from enhanced parameter learning with increased patience. Different with the indentation recognition, the wear recognition model requires more features when using only a single convolutional layer, with the highest accuracy of 97.92% using 16 kernels. When the 1D CNN model adopts a dual convolutional layer and dual FC layer structure, the model performs the best when the number of convolutional kernels in each layer is 4 and 8.

5. Discussion

5.1 The comparison between two recognition models

Comparing the two recognition models in Section 4.2 and 4.3, when the model structure is the same, the classification accuracy of the two models is different, while the accuracy of the indentation recognition model is higher. As per the previous researches, ultrasound has more advantages in wear recognition, because it is difficult to distinguish fault signals from the deformed surface of an indentation. Intuitively speaking, 1D CNN should have performed better in wear recognition, but the results were contrary to expectations.

This is potentially led by the complexity of failures in wear recognition dataset. The samples used to train wear recognition models come from various testing conditions, such as artificial damages, the damages from dry-running/severe conditions, or long-term in-situ measurements. The samples of the indentation recognition model only come from one type of damage (indented surface). It can be inferred that in the wear recognition dataset, due to the complexity or diversity of various damage signals, the undamaged surfaces are easier to identify. In the indentation recognition dataset, the signals from the indentation are extremely similar to the undamaged surface signals, making them more difficult to be identified.

Table 7 compares the classification results of SVM and LSTM models on the datasets in Section 4.2 and 4.3, also split into training, validation and test datasets. Regarding the SVM model, the accuracy of three type of features, time-domain features, frequency-domain features, and energy bands of wavelet packet decomposition (using Daubechies 4 basis), were first compared. Finally, six time-domain features, which are mean, variance, standard deviation, root mean square value, mean absolute value, and energy of the ultrasound signal were selected as feature vectors, and then send into SVM training. The linear kernel function was used, and the regularization parameters of the indentation model and wear model were 1.29 and 4.64, respectively. The LSTM model architecture consists of two unidirectional LSTM layers with an input dimension of 1, a hidden dimension of 64, and a dropout rate of 0.2 between layers. The undamaged surface is referred as negative, while a surface with indentation or wear is positive.

Table 7. A Comparison between 1D CNN, LSTM and SVM algorithm on indentation and wear datasets.

	Indentation Recognition				***Wear Recognition***			
	Accuracy	*Precision*	*Recall*	*F1-Score*	*Accuracy*	*Precision*	*Recall*	*F1-Score*
1D-CNN	*98.96%*	*0.9934*	*0.9901*	*0.9917*	*99.87%*	*1*	*0.9977*	*0.9988*
LSTM	*85.83%*	*0.8415*	*0.7667*	*0.8023*	*99.57%*	*0.9952*	*0.9971*	*0.9952*
SVM	*78.12%*	*0.7376*	*0.6047*	*0.6645*	*79.95%*	*0.7525*	*0.8443*	*0.7957*

From Table 7, it can be observed that regardless of the classification algorithm used, the model always performs well on the wear recognition dataset, that is, a surface damage can be easier identified. Although all classification methods may experience false positives and false negatives on the indentation recognition dataset, 1D CNN can still effectively reduce the appearance of false positives and false negatives. This will be beneficial to in-situ ultrasound testing, as deformations can be identified instead of being considered as undamaged surfaces.

Additionally, as shown in Table 5 and 6, as the number of FC layers increases, the rise of accuracy is not that significant. In the meantime, using more convolutional layers and more kernels have shown a better improvement. Taking indentation recognition as an example, when using only a single convolutional layer, four kernels are enough for feature extraction, while the performance will be better if an extra convolutional layer is applied. Therefore, considering the accuracy and efficiency, a structure of two convolutional layers and one FC layer would be the best choice, while the kernels per layer would be four and sixteen.

5.2 The features studied from the ultrasound signals

1D CNN is suitable for capturing local features of ultrasound signals and it can potentially extract some unknown high-dimensional features. In addition, the "convolution" operation in 1D CNN is similar to the translation and scaling in traditional wavelet analysis. Figure 14 shows the shape of trained kernels and the extracted features from ultrasound signal.

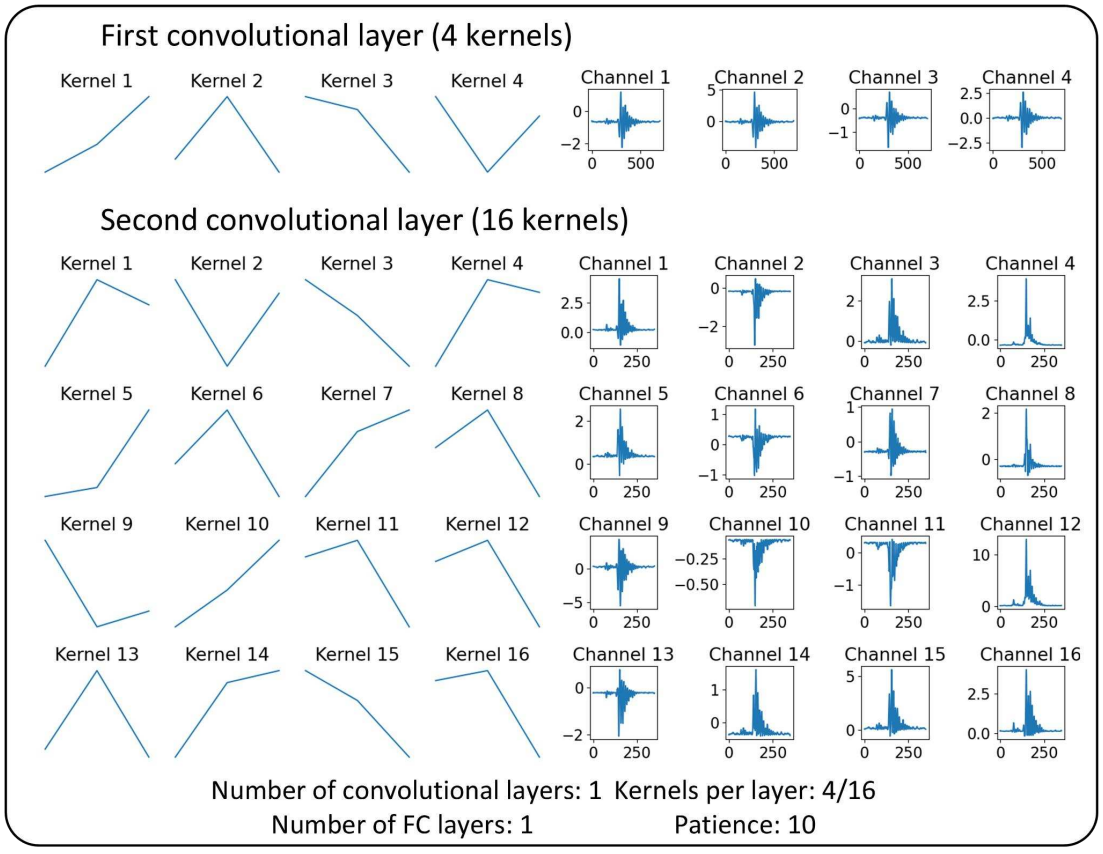

Figure 14. The convolution kernels and extracted features of the indentation recognition model. Two convolutional layers, 4/16 convolution kernels, one FC layer.

It is worth mentioning that in the indentation recognition model, after increasing the number of convolution layers, the four convolution kernels in the first layer still maintain their

original shape. This means that for the classification of indentation, four convolutional kernels can basically achieve the classification function. For the wear recognition model, due to the diversity of the wear surface itself, it is necessary to increase the number of convolution kernels or the complexity of the model to achieve effective feature extraction and classification. Considering the shape of kernels on the first convolutional layer, Kernel 1 and 3 are used to capture the rising and falling trends, while Kernel 2 and 4 are used to capture the peak and valley.

Moreover, regarding the output of first convolutional layer, the phase of Channel 1 and 2 are the same, but there is a bias along y-direction, while the amplitudes are different as well. The signals of Channel 3 and 4 are in reverse phase compared to Channel 1 and 2. Therefore, it can be speculated that the intrinsic logic of identifying a surface damage may be related to the phase change of ultrasound reflections. This may explain the superposition of the reflected signals from indentation, or other types of surface damage, but it still needs to be further analyzed by combining a large number of signals. For the high-dimensional signals output by the second convolutional layer, further in-depth research is also required.

By comparing the results of ultrasound testing with the classification results of 1D CNN, on one hand, the 1D CNN model can effectively identify the indented surface, while ultrasound testing is difficult to quantitatively analyze this complex and superposed reflection signal. On the other hand, for determining whether the surface is damaged, 1D CNN is applicable to the bearings and coatings of various materials and dimensions. For example, changes in the coating material only affect the phase and amplitude of the reflected signal from the deformed or indented area, the 1D CNN structure can still capture the local details or changes of these reflected signals. From these two perspectives, 1D CNN has the potential to be an invaluable auxiliary tool for ultrasound in-situ monitoring, enhancing diagnostic capabilities particularly in complex detection scenarios.

6. Conclusion

In this article, a dynamic wear process was explained initially, to provide the background of using active ultrasound to measure the early-state wear. Then, the numerical simulation was presented to demonstrate the ultrasound behaviour at the indentation, as well as the early-state wear. The 22 MHz ultrasound sensors were used for detecting indentations, which had the similar profile with the early-state wears. Five samples were instrumented for the test, and each sample was processed with three indentations on its surface, with loads of 50 N, 100 N and 150 N respectively. For the indentation generated by 150 N load, ultrasound measurement can obtain the average and minimum thickness of the coating, but for the indentation generated by 100 N load, the minimum thickness of some samples cannot be detected. For the indentation generated by 50 N load, ultrasound can only detect an average thickness of about 50 μm.

Afterwards, the indentation recognition model was established and the results showed that the model could effectively identify the indentation on coating materials. A wear recognition model based on 1D CNN was proposed based on the data of aluminum-alloy coated samples with various types of surface damages. The feasibility of 1D CNN in identifying ultrasound signals was tested, proving that 1D CNN can identify whether there is any surface damage to the coating. The results indicate that 1D CNN is expected to be an auxiliary method for further ultrasound in-situ monitoring of the bearing coating materials.

Acknowledgements

The authors would like to acknowledge the financial support of the Daido Metal Co whofunded this work. RDJ would also like to acknowledge the financial support of the Engineering and Physical Sciences Research Council through his fellowship on Tribo-Acoustic Sensors EP/N016483/1.

Reference

[1] Patrick G. Swan, "Studies in plain bearing failures," *TRIBOLOGY & LUBRICATION TECHNOLOGY*, vol. 62, no. 10, pp. 28–31, 2006.

[2] F. S. Silva, "Analysis of a vehicle crankshaft failure," *Eng Fail Anal*, vol. 10, no. 5, pp. 605–616, 2003, doi: 10.1016/S1350-6307(03)00024-4.

[3] G. H. Isaac, J. Thompson, S. Williams, and J. Fisher, "Metal-on-metal bearings surfaces: Materials, manufacture, design, optimization, and alternatives," *Proc Inst Mech Eng H*, vol. 220, no. 2, pp. 119–133, Feb. 2006, doi: 10.1243/095441105X68953.

[4] P. Sateesh Kumar *et al.*, "A study of surface fatigue wear and influence of contaminated lubricant in journal bearing system using tribological and vibration analyses," *Proceedings of the Institution of Mechanical Engineers, Part E: Journal of Process Mechanical Engineering*, Feb. 2024, doi: 10.1177/09544089241233119.

[5] C. Ates, T. Höfchen, M. Witt, R. Koch, and H.-J. Bauer, "Vibration-Based Wear Condition Estimation of Journal Bearings Using Convolutional Autoencoders," *Sensors*, vol. 23, no. 22, p. 9212, Nov. 2023, doi: 10.3390/s23229212.

[6] L. Wu, I. Palamarciuc, R. Bajwa, Y. Zhang, and R. S. Dwyer-Joyce, "In-situ ultrasonic shear wave sensing of thin metallic coatings on journal bearing shells," *Friction*, Aug. 2025, doi: 10.26599/FRICT.2025.9441160.

[7] F. Hu, C. Ning, and W. Ouyang, "Ultrasonic in-situ measurement method and error analysis of wear of PEEK water-lubricated bearing materials," *Measurement*, vol. 214, p. 112822, Jun. 2023, doi: 10.1016/j.measurement.2023.112822.

[8] F. A. Davis and T. S. Eyre, "Wear of plain bearing materials with particular reference to role of soft phases," *Materials Science and Technology*, vol. 7, no. 8, pp. 746–756, Aug. 1991, doi: 10.1179/mst.1991.7.8.746.

[9] H. Brunskill, P. Harper, and R. Lewis, "The real-time measurement of wear using ultrasonic reflectometry," *Wear*, vol. 332–333, pp. 1129–1133, May 2015, doi: 10.1016/j.wear.2015.02.049.

[10] L. Wu, I. Palamarciuc, R. Bajwa, Y. Zhang, and R. Dwyer-Joyce, "The wear measurement of journal bearing coatings that are poor reflectors using ultrasound analytical signals," *Wear*, vol. 572–573, p. 206052, Jul. 2025, doi: 10.1016/j.wear.2025.206052.

[11] P. Dou *et al.*, "Ultrasound enabled simultaneous measurement of coating wear depth and lubricant film thickness in a sliding bearing," *Measurement*, vol. 240, p. 115602, Jan. 2025, doi: 10.1016/j.measurement.2024.115602.

[12] L. Wu, I. Palamarciuc, R. Bajwa, Y. Zhang, and R. Dwyer-Joyce, "An in-situ wear measurement instrumentation for thin metallic bearing coatings using high frequency ultrasound," *Tribol Int*, vol. 214, p. 111267, Feb. 2026, doi: 10.1016/j.triboint.2025.111267.

[13] V. G. Salunkhe and R. G. Desavale, “An Intelligent Prediction for Detecting Bearing Vibration Characteristics Using a Machine Learning Model,” *J Nondestruct Eval Diagn Progn Eng Syst*, vol. 4, no. 3, Aug. 2021, doi: 10.1115/1.4049938.

[14] F. Piltan *et al.*, “Strict-Feedback Backstepping Digital Twin and Machine Learning Solution in AE Signals for Bearing Crack Identification,” *Sensors*, vol. 22, no. 2, Jan. 2022, doi: 10.3390/s22020539.

[15] E. T. Chelmiah, V. I. McLoone, and D. F. Kavanagh, “Remaining Useful Life Estimation of Rotating Machines through Supervised Learning with Non-Linear Approaches,” *Applied Sciences (Switzerland)*, vol. 12, no. 9, May 2022, doi: 10.3390/app12094136.

[16] D. T. Hoang and H. J. Kang, “Rolling element bearing fault diagnosis using convolutional neural network and vibration image,” *Cogn Syst Res*, vol. 53, pp. 42–50, Jan. 2019, doi: 10.1016/j.cogsys.2018.03.002.

[17] M. Bertocco *et al.*, “Roller Bearing Failures Classification with Low Computational Cost Embedded Machine Learning,” in *2022 IEEE International Workshop on Metrology for Automotive, MetroAutomotive 2022 - Proceedings*, Institute of Electrical and Electronics Engineers Inc., 2022, pp. 12–17. doi: 10.1109/MetroAutomotive54295.2022.9855137.

[18] F. König, G. Jacobs, A. Stratmann, and D. Cornel, “Fault detection for sliding bearings using acoustic emission signals and machine learning methods,” *IOP Conf Ser Mater Sci Eng*, vol. 1097, no. 1, p. 012013, Feb. 2021, doi: 10.1088/1757-899x/1097/1/012013.

[19] T. H. T. Nguyen, N. V. Phạm, and Q. H. Hoàng, “Bearing fault diagnosis by machine learning and deep learning-based models: A comparative study applying for HUST bearing dataset,” *Journal of Military Science and Technology*, vol. 103, pp. 31–39, May 2025, doi: 10.54939/1859-1043.j.mst.103.2025.31-39.

[20] L. Jing, M. Zhao, P. Li, and X. Xu, “A convolutional neural network based feature learning and fault diagnosis method for the condition monitoring of gearbox,” *Measurement (Lond)*, vol. 111, pp. 1–10, Dec. 2017, doi: 10.1016/j.measurement.2017.07.017.

[21] S. Kiranyaz, O. Avci, O. Abdeljaber, T. Ince, M. Gabbouj, and D. J. Inman, “1D convolutional neural networks and applications: A survey,” *Mech Syst Signal Process*, vol. 151, p. 107398, Apr. 2021, doi: 10.1016/j.ymssp.2020.107398.

[22] K. Zhang, Y. Chen, S. Gao, and Y. Zhang, “Research on hybrid fault diagnosis method for rolling bearings,” *Journal of the Brazilian Society of Mechanical Sciences and Engineering*, vol. 47, no. 11, p. 596, Nov. 2025, doi: 10.1007/s40430-025-05885-3.

[23] E. Muratbakeev, D. Novak, and Y. Kozhubaev, “Investigation of Industrial Bearing Fault Diagnosis Based on 1D-Cnn-Lstm,” in *2025 International Conference on Industrial Engineering, Applications and Manufacturing (ICIEAM)*, IEEE, May 2025, pp. 1059–1067. doi: 10.1109/ICIEAM65163.2025.11028381.

[24] A. Wan *et al.*, “Fault diagnosis of air conditioning compressor bearings using wavelet packet decomposition and improved 1D-CNN,” *Next Energy*, vol. 9, p. 100424, Oct. 2025, doi: 10.1016/j.nxener.2025.100424.

[25] L. Eren, “Bearing fault detection by one-dimensional convolutional neural networks,” *Math Probl Eng*, vol. 2017, 2017, doi: 10.1155/2017/8617315.

[26] A. Vencl and A. Rac, “Diesel engine crankshaft journal bearings failures: Case study,” *Eng Fail Anal*, vol. 44, pp. 217–228, Sep. 2014, doi: 10.1016/j.engfailanal.2014.05.014.

[27] R. Lewis and U. Olofsson, “Basic tribology of the wheel–rail contact,” in *Wheel–Rail Interface Handbook*, Elsevier, 2009, pp. 34–57. doi: 10.1533/9781845696788.1.34.

[28] A. Abdelbary, “Polymer tribology,” in *Wear of Polymers and Composites*, Elsevier, 2014, pp. 1–36. doi: 10.1533/9781782421788.1.

[29] O. Abdeljaber, O. Avci, S. Kiranyaz, M. Gabbouj, and D. J. Inman, “Real-time vibration-based structural damage detection using one-dimensional convolutional neural networks,” *J Sound Vib*, vol. 388, pp. 154–170, Feb. 2017, doi: 10.1016/j.jsv.2016.10.043.

[30] Z. Xu, J. Zhao, Y. Yu, and H. Zeng, “Improved 1D-CNNs for behavior recognition using wearable sensor network,” *Comput Commun*, vol. 151, pp. 165–171, Feb. 2020, doi: 10.1016/j.comcom.2020.01.012.